Effects of relative humidity and phase on the molecular detection of nascent sea spray aerosol using extractive electrospray ionization

Samantha M. Kruse,[1] Paul R. Tumminello,[1] Alexia N. Moore,[1] Christopher Lee,[2] Kimberly A. Prather,[1,2] and Jonathan H. Slade[1*]

[1]Department of Chemistry & Biochemistry, University of California San Diego, La Jolla, CA, 92093, United States; [2]Scripps Institution of Oceanography, University of California San Deigo, La Jolla, CA, 92093, United States

ABSTRACT: Online mass spectrometry techniques, such as extractive electrospray ionization time-of-flight mass spectrometry (EESI-TOF), present an attractive alternative for analyzing aerosol molecular composition due to reduced aerosol sample collection and handling times and improved time resolution. Recent studies show a dependence of EESI-TOF sensitivity on particle size and mixing state. This study measured authentic sea spray aerosol (SSA) components generated during a phytoplankton bloom, specifically glycerol, palmitic acid, and potassium ions. We demonstrate temporal variability and trends dependent on specific biological processes occurring in seawater. We found that the EESI-TOF sensitivity, after adjusting for pressure variations at the inlet and normalizing to the reagent ion, critically depends on the sample's relative humidity. Relevant SSA species exhibited heightened sensitivity at an elevated relative humidity near the deliquescence relative humidity of sea salt and poorer sensitivity with sparse detection below the efflorescence relative humidity. Modeling the reagent ion's diffusive depth demonstrates that the sample aerosol particle viscosity governs the relative humidity dependence because it modulates the distance the reagent ion diffuses and reacts with components in the particle bulk. Furthermore, the particle's stickiness and coagulation efficiency with the electrospray droplets increase at higher relative humidity. The effects of particle size and mixing state are discussed, revealing improved sensitivity of phase-separated components present along the particle surface. This work highlights the importance of the particle phase state in detecting and quantifying molecular components within authentic and complex aerosol particles and the utility of EESI-TOF for measuring SSA composition.

INTRODUCTION

Sea spray aerosols (SSA) play a crucial role in the climate system by influencing the global radiative budget through the direct and indirect scattering and absorption of solar and terrestrial radiation.[1-6] SSA constitutes the most abundant aerosol by mass in the atmosphere alongside mineral dust,[7, 8] with an estimated global production rate ranging from 3 to 70 Pg yr^{-1}.[8, 9] This mass significantly surpasses anthropogenic aerosols and contributes substantially to the global aerosol burden, providing considerable cloud condensation nuclei (CCN).[10] Atmospheric models commonly parameterize SSA as pure sea salt.[11, 12] Yet, they are far more chemically and physically complex, encompassing varying mixtures of dissolved and crystalline inorganic salts,[13] dissolved and particulate organic carbon,[14, 15] and whole cells.[16] The proportions of these components vary with particle diameter due primarily to their production method via bubble bursting.[17-19] Though organic matter may not dominate the total SSA mass, it can constitute a significant portion of SSA particles smaller than 1 μm in the ambient marine atmosphere, with film droplets that are primarily organic carbon constituting ~57% of the number concentration of submicron SSA.[17, 18, 20] Moreover, studies show a higher organic carbon mass fraction in ultrafine (<0.1 μm) SSA, with purely organic SSA particles exceeding the SSA particles comprised only of sea salts or sea salts mixed with organic carbon.[17, 18, 21, 22] Identified organic molecules in SSA include free and polysaccharides,[23] lipids and fatty acids,[24, 25] and amino acids.[26, 27] Organic matter can modulate water uptake and the CCN activity of SSA.[4, 28, 29] Therefore, characterizing the molecular composition of SSA and factors such as biological activity altering the organic carbon proportion of SSA particles is crucial for better understanding their indirect radiative effects, the least understood aspect of global radiative forcing.[30]

Several techniques have contributed to the growing knowledge of SSA composition. For example, liquid chromatography coupled with high-resolution mass spectrometry (HRMS) can detect individual organic molecules and elemental ratios in SSA.[31-33] While highly sensitive, these measurements face challenges such as long sample collection times (between 5 and 12 hours)[34] needed to obtain sufficient particulate mass for detection, storage, incubation, sample extraction, and derivatization.[35, 36] Techniques like Raman[37, 38] and IR spectroscopy[39, 40] focus on identifying specific functional groups and compound classes. These methods can be coupled with microscopy to determine inter- and intra-particle chemical variability with high chemical specificity for the particle's surface,[40, 41] but focus on a single particle at a time. While such measurements have been critical to understanding SSA composition, in dynamic marine environments with rapidly changing conditions such as variations in water biological activity, air temperature, relative humidity, air mass history, and wave break conditions occurring on short timescales, online methods become indispensable for accurately capturing the temporal variability in SSA composition. Currently, online techniques, such as

aerosol mass spectrometry (AMS) and aerosol time-of-flight mass spectrometry (ATOFMS), have been employed for size-dependent chemical composition analysis of SSA particles,[42, 43] but extensive molecular fragmentation prevents unambiguous detection of individual molecules in SSA, necessitating softer ionization approaches.

Extractive electrospray ionization time-of-flight mass spectrometry (EESI-TOF)[44] is a promising yet untested online technique for analyzing SSA chemical composition. During EESI, aerosol components are extracted following collision and coalescence between the aerosol and a charged solvent spray (electrospray). Sample molecules are ionized based on their binding affinity with a reagent ion in the electrospray droplet (commonly Na^+), and the ionized sample molecules are then detected downstream after being heated and evaporated into the gas phase.[45] With the entire EESI process occurring in a fraction of a second, this technique enables high temporal resolution aerosol chemical composition measurements. Operating in positive mode ionization with Na^+, EESI-TOF has achieved detection limits of 1-10 ng m^{-3} or even lower for some organic molecules.[44-46] While applied in various field studies,[47-51] its application to SSA has been limited, with only one study from this lab conducted thus far.[52]

The exact EESI mechanism is still debated, and although there have been a few studies employing single-component organic aerosols and internally mixed binary-component organic/inorganic aerosols generated in the lab that examined the effects of particle size,[53] component volatility,[54] relative humidity (RH),[44] and particle organic coating thickness[55] on EESI extraction efficiency, none have considered such effects on aerosols sampled in the field or authentic SSA. SSA particles adopt different phase states (viscosities), morphologies, and mixing states that change with RH and biological activity.[22, 52, 56-58] Changes in RH can induce complex multistep phase transitions in SSA.[56] Such changes likely affect the extraction and ionization efficiencies of EESI, e.g., by altering the coagulation efficiency between the aerosol sample and electrospray droplets and the bulk diffusion rates of ions and molecules within the droplet-aerosol mixture. To our knowledge, factors such as particle viscosity and RH-induced phase transitions have not been characterized in terms of how they affect EESI.

This study investigates the effects of sample RH (spanning a range of 20% to 75% near the sea salt efflorescence and deliquescence RH, respectively) and subsequent changes to particle viscosity on the molecular detection of components in authentic SSA produced while inducing a phytoplankton bloom in natural seawater in a wave flume. The study also aims to provide insights into the temporal variations in specific SSA molecular components during the bloom, emphasizing the method's capability to detect and track SSA compositional changes with higher temporal resolution and softer ionization than previous techniques throughout a bloom cycle. This work underscores the importance of the particle phase state in the molecular detection of components by EESI in authentic SSA, which needs to be considered in other ambient aerosol measurements that use EESI.

EXPERIMENTAL SECTION

SSA Generation and Biological Activity Measurements

This study was conducted as part of the Sea Spray Chemistry and Particle Evolution (SeaSCAPE) study in 2019 with the National Science Foundation Center for Aerosol Impacts on Chemistry of the Environment (NSF-CAICE). Comprehensive details of the study can be referred to in previous works,[32, 34, 40, 41, 52, 59-61] with a brief overview provided here. Water was sampled from the Scripps Pier in La Jolla, CA (32° 52' 01.0" N, 117° 15' 25.7" W) on 7/23. The water was filtered using 50 μm Nitex nylon mesh (Flystuff; Cat # 57-106) to remove larger biological species. This water was placed into the 11,800 L, 33 m-long glass tank equipped with fluorescent lamps along the outer walls and a moving paddle to simulate a diurnal solar cycle and generate SSA through wave breaking. A phytoplankton bloom was induced by spiking the water with f/2 growth media and sodium metasilicate. This work focuses explicitly on SSA measurements during the third bloom between 7/31 and 8/9, which generated the largest biomass. Biological activity was monitored by measuring chlorophyll-a concentration via continuous fluorescence (ESP),[62] an indication of algal biomass, bacterial cell counts with a Liquid Spot Sampler (SS110A, Aerosol Devices Inc) and flow cytometry, and dissolved organic carbon (DOC) concentrations with a Shimadzu TOC-V_{CSH} catalytic combustion oxidation instrument.

Sampling Apparatus and Conditions

The sampling apparatus and conditions followed the details outlined in Tumminello et al., 2021.[52] Briefly, filtered air was supplied to the wave flume's headspace to prevent outside contamination, and the headspace air was drawn through one silica gel diffusion dryer and into our sampling setup at a flow rate of 5 L min^{-1}. A Pyrex flow tube (inner diameter of 5 cm and 50 cm long) facilitated the mixing and equilibration of particles at the tube's RH, adjusted by varying zero air (747-30, AADCO) flows through a bubbler containing pure water or a "dry" bypass sampling line. These RH values were measured by an inline RH/temperature sensor (Sensirion AG). The sample flow was split for particle size and composition analysis, passing through a honeycomb-type activated charcoal denuder to remove volatile hydrocarbons before entering the mass spectrometer inlet, as shown in Fig. 1. Two two-way valves directed the flow either directly into the inlet or through two particle filters connected in series (HEPA Capsule Versapor, 99.97% efficiency for 0.3 μm) for a background, or "blank" measurement. Filter blanks were taken at the start of every measurement period at four flow settings to modulate RH (20 min total, 5 min each). Then the sampling and long RH cycles began (1 hr at each setting, four settings total), also shown in Fig. S1. SSA size distributions were measured every two minutes with a Brechtel scanning electrical mobility sizer (SEMS; Model 2100; size range of 5 nm to 850 nm across 100 size bins). Measurements occurred in approximately three to four (dependent on start time) subsequent 4-hour cycles overnight (8-11 P.M. to 7-8:30 A.M. local time), systematically adjusting between four RH regimes within a cycle from a maximum RH of ~75% to a minimum RH of ~20%, covering a range that extended to the deliquescence RH (DRH) (~75%) and below the efflorescence RH (ERH) (~44%) of NaCl. We categorized RH into four regimes depending on the wet-to-dry flow ratio: 20-35%, 35-50%, 50-65%, and 65-75%.

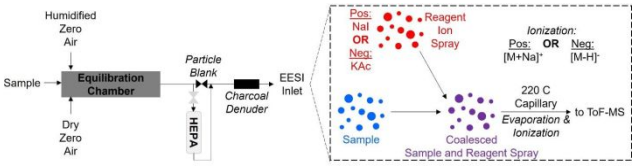

Figure 1. EESI-TOF sampling apparatus and visualization of the ionization mechanism.

EESI-TOF Description

The nascent SSA molecular composition was measured using an extractive electrospray ionization time-of-flight mass spectrometer (EESI-TOF; Aerodyne Research Inc. and Tofwerk AG). EESI involves exposure of the aerosol sample to suspended electrospray droplets, resulting in a signal proportional to the mass concentration of components in the aerosol phase.[44, 47, 48, 50, 52, 63, 64]The reagent ion spray was generated by passing the reagent solution through a 365 µm OD fused silica capillary (IDEX Health and Science, LLC) at a pressure of 350 mbar. It was charged at −2500V in negative mode and +2500V in positive mode. The reagent solution for negative mode consisted of 50% (by mass) H_2O (18 mΩ, Millipore Synergy System) and 50% acetonitrile (≥99.95%, Fisher Chemical) spiked with 100 ppm potassium acetate (99%, Sigma-Aldrich), resulting primarily in ionization by deprotonation $[M-H]^-$. In positive mode, the reagent solution consisted of 50% acetonitrile (≥99.95%, Fisher Chemical) and 50% H_2O spiked with 100 ppm sodium iodide (99%, Sigma-Aldrich), which ionized the sample by clustering with sodium $[M+Na]^+$. Negative and positive mode EESI-TOF measurements were conducted, but only positive mode results are described here because of their broader coverage throughout the measurement period. The aerosol was sampled at 1 liter per minute (LPM), mixed with the reagent ion spray, and heated to 220 °C before detection by the TOF mass analyzer.[46]

Mass Spectra Data Processing

The mass spectra were processed using Tofware (Version 3.3.0, Aerodyne Research Inc. and Tofwerk AG) in IGOR 9 (Wavemetrics). Files with 1-second time resolution were averaged in 60-second increments before further high-resolution analysis. After data processing, there was <10 ppm error in the mass calibration and a resolution of ~5000 m/Δm in negative mode for m/z=59.013853 (CH_3COO^-) and ~5500 in positive mode for m/z=22.989221 (Na^+). Chemical formulae were determined using a pre-determined peak list based on compounds previously identified in SSA (Table S1) and the formula generator developed by Stark et al. 2015.[65] The generator allowed for all combinations of C, H, O, and N with m/z in the range from 50 to 400, with maximum oxygen-to-carbon ratios (O:C) of 2, double bond equivalences (DBE) from 0 to 1, and minimum hydrogen-to-carbon ratios (H:C) of 0.5.[65, 66] Due to some clustering between molecular ions and the acetonitrile organic solvent, which could flag as false positives for CHON compounds when they are possibly CHO compounds clustered with acetonitrile, all nitrogen-containing elemental formulae were omitted from the peak list, except for those with the same formulae as amino acids previously measured in SSA.[27]

Peaks were identified as present if their mass accuracy was within 15 ppm and intensities were above the limit of detection, determined by the area near the peak, as done in Lopez-Hilfiker et al. 2019.[44] It is important to note that some volatile components that transmit through the charcoal denuder and break through the particle filters used for blank measurements can dissolve into or become solvated in the electrospray and lead to elevated background levels.[48] The filters and denuder were new as of the start of the study and regularly cleaned by flushing with dry zero air and, for the charcoal denuder, baking it in an oven at 150 °C. Detected molecular ions were filter-blank subtracted and normalized to the background Na^+ reagent ion intensity at the corresponding RH without further corrections, mitigating interferences from gas breakthrough, Na^+ in SSA, and accounting for potential sensitivity differences with varying RH.

RESULTS AND DISCUSSION

Temporal Trends and Variability in Measured SSA Components with Changing Seawater Biology

This section elucidates the temporal trends and variability in tracer components within nascent SSA measured by EESI-TOF. We focus on the temporal behavior and enrichment during a controlled phytoplankton bloom of K^+, palmitic acid, and glycerol, which are representative components in nascent SSA that depend on seawater biological activity.[23, 24, 67, 68]

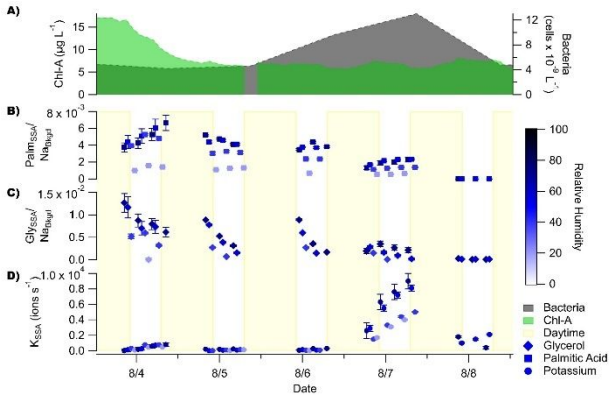

Figure 2. Time series of (A) chlorophyll-a concentrations in µg L^{-1} (green) and bacterial cell counts in cells x 10^{-9} L^{-1} (gray). Hourly-averaged normalized intensities of (B) palmitic acid (squares) (C) glycerol (diamonds), and (D) potassium (circles). The blue scale refers to the average relative humidity of the incoming sample aerosol within the hourly-averaged period. The yellow shading represents the "daytime" hours, defined by the times when the lights outside the flume were on. For B and C, the signal intensities were background-subtracted and normalized to the background Na^+ reagent ion signal at the same relative humidity as the sample. For D, the signal intensity of K^+ was taken directly because it does not depend on the Na^+ reagent ion. Error bars represent one standard deviation from the mean hourly-averaged data.

Marine biological activity can be assessed through various biological markers, as depicted in Fig. 2A. This section provides a brief overview of the results concerning these markers, with a more comprehensive analysis in Sauer et al. 2022.[34] Chlorophyll-a is the primary marker for monitoring phytoplankton growth, as they produce chlorophyll-a to capture sunlight energy. While phytoplankton can generate different types of chlorophyll, measurements of chlorophyll-a remain the most reliable indicator of overall phytoplankton growth.[69] Diatoms (mainly *Skeletonema* sp. and *Cylindrotheca*

sp.) and diatom aggregates (mostly *Cylindrotheca* sp. and *Navicula* sp.) dominated the phytoplankton communities in this study.[34] Following the phytoplankton bloom, there was an extended period of senescence after 8/5, succeeded by a surge in bacteria, as confirmed by bacterial cell counts, a characteristic feature of post-bloom conditions established in prior research.[34, 70] Table 1 shows the r^2 values for each identified compound versus the chlorophyll-a concentration and bacterial cell counts, with the correlation plots in Fig. S5.

Table 1. Correlation coefficients (R^2 values) for the linear regression analysis of chlorophyll-a and bacteria cell counts with palmitic acid, glycerol, and potassium.

	Palmitic Acid	Glycerol	Potassium
Chlorophyll-A	0.06	0.48	0.11
Bacteria	0.05	0.11	0.62

Figure 2B shows the temporal variability in $C_{16}H_{32}O_2Na^+$ (*m/z*=279.229451), tentatively identified as palmitic acid, the predominant saturated fatty acid in nascent SSA at concentrations between 20 and 214 ng m^{-3}.[14, 24] The highest palmitic acid levels in SSA coincided with the end of the chlorophyll-a peak on 8/4, diminishing as the bacterial levels increased. It is unclear if the palmitic acid levels in nascent SSA were greater in earlier stages of the phytoplankton bloom before the positive mode EESI-TOF measurements, but studies show an increase in fatty acid concentration within SSA after nutrients are exhausted during a phytoplankton bloom.[24, 25] In a diatom-dominated bloom, palmitic acid and other 16-carbon fatty acids are produced by the phytoplankton,[71] potentially increasing palmitic acid levels in SSA near the chlorophyll-a peak's end. Following the peak, palmitic acid levels decreased, then decreased more rapidly as the bacteria grew on 8/6 and 8/7. This decline may result from its usage by bacteria, as all bacteria can incorporate exogenous fatty acids for use in the β-oxidation cycle to yield acetyl-coenzyme A, which the bacteria can then use to make phospholipids to build the cell membrane.[72] The decreasing trend in palmitic acid across the bloom did not align with the total SSA volume, surface area, or number concentration trends, which remained relatively stable except when the lamps were on (Fig. S6). Additionally, the concentrations of palmitic acid did not strongly correlate with chlorophyll-a or bacteria (r^2=0.06 and 0.05, respectively). Although previous work suggests a diel cycle in SSA production,[73-76] our study lacked sufficient measurements during lamp-on periods to identify any diurnal trend in SSA composition.

Figure 2C shows the temporal variability in $C_3H_8O_3Na^+$ (*m/z*=115.036565), tentatively identified as glycerol due to it having no naturally occurring structural isomers, its prevalence in marine biota,[77] and SSA.[78] Glycerol, a small saccharide and the backbone of triglycerides and phospholipids, showed decreasing levels in nascent SSA from 8/4 to 8/8. However, unlike palmitic acid, glycerol exhibited consistently higher signals at the start of the night, decreasing through the night during all five nighttime measurement periods. Glycerol, a byproduct of photosynthesis,[79] can be exuded by phytoplankton into surrounding water, varying in quantity with phytoplankton type.[80-83] As photosynthesis stops once the wave flume lights are turned off, glycerol levels decrease. This could explain the glycerol signal decay throughout the nighttime sampling period and the better correlation between glycerol and chlorophyll-a (r^2=0.48), as chlorophyll-a reflects the photosynthetically active phytoplankton abundance. Additionally, bacteria can metabolize glycerol for energy, potentially explaining the near-zero glycerol signal by the end of the bloom following the bacterial spike on 8/7.[84]

Figure 2D presents temporal variability and trends in K^+ in SSA (detected at *m/z*=38.963158), with K^+ confirmed by its isotopic abundance in the mass spectra (Fig. S7). K^+ is known to be enriched relative to Na^+ in SSA compared to seawater.[17, 23] The signal remained relatively low and stable immediately following the bloom but subsequently increased, coinciding with gradual bacterial growth after 8/5 (r^2=0.62). A similar trend in K^+ enrichment relative to Na^+ was observed in Jayarathne et al. 2016,[23] coinciding with the maxima in chlorophyll-a and bacterial cell counts. This enrichment was attributed to the complexation of cations with dissolved organic carbon components at the sea surface, including oligo/polysaccharides selectively transferred in SSA. Such cation enrichment has been observed in other studies.[85, 86] While Mg^{2+} and Ca^{2+} in SSA are expected to be enhanced alongside K^+, they were not detected in this study, possibly because the TOF mass analyzer was tuned to Na^+-ion adducts and not to doubly charged species like Mg^{2+} and Ca^{2+}.

Local changes in water pH could influence these observations, as pH can affect complexation.[87, 88] Flynn and Mitra et al., 2023, demonstrated that phytoplankton activity can impact local pH, where growth leads to increased pH due to CO_2 uptake, and subsequent heterotrophic consumption results in decreased pH.[89] Throughout this phytoplankton bloom, the average pH of the bulk water increased from ~7.9 on 7/31 to as high as ~8.3 at peak chlorophyll-a concentration on 8/4 and 8/5, followed by a subsequent decrease in pH, as shown in Fig. S3. The pH of the sea surface microlayer (SSML) remained relatively stable between 7/31 and 8/5, decreasing following the bloom from a high of ~8.0 on 8/5 to a low of ~7.7 as the bacteria grew in. Hakim et al. 2019 indicated that pH can influence the complexation of cations with DOM, where an increase in pH, especially above the pKa of DOM, enhances binding between anionic forms of the organic carbon and divalent cations.[90] Considering that previous work shows 60% of marine DOM exhibits carboxylic-like pKa values of 3.6 and 4.8,[87] we conjecture that the increase in K^+ in SSA coinciding with the peak in bacteria cell counts could be due to a smaller proportion of K^+ bound to anionic forms of DOM in the SSML at the lower pH, effectively "releasing" the carbon-bound K^+ and forming free K^+ in SSA, which becomes detectable by EESI.

Relative Humidity Effects

Substantial variations in the EESI-TOF intensity for specific ions (normalized to the background reagent Na^+) were noted in response to changes in the sample RH, as shown in the color scale of Fig. 2. We illustrate this further in Fig. 3A for palmitic acid during a representative measurement cycle, showing a significant decrease in the reagent ion-normalized signal as the RH was stepped down from ~70% to ~20%. As shown in Fig. S4, changes in intensity were evident in nearly all signals associated with SSA with varying RH, with less signal variability (i.e., relative error) for ions at lower m/z and

elevated RH. For the majority, though not all, of the identified MS peaks, intensities were prominent under elevated RH, while most approached background levels or were undetected (i.e., below background) at RH < 40%.

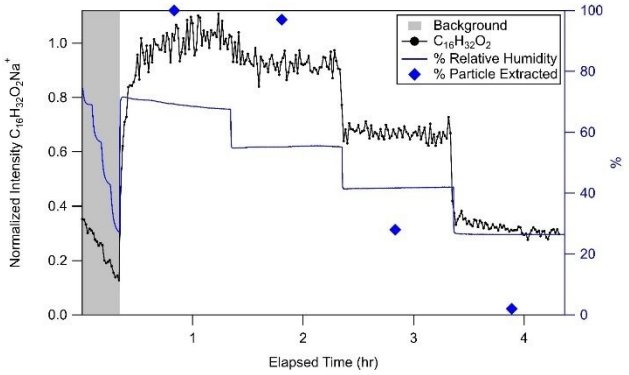

Figure 3. (A) Example temporal profile of the normalized $C_{16}H_{32}O_2Na^+$ (palmitic acid) intensity during one measurement cycle with changing relative humidity (black). The background measurement period is highlighted in the gray-shaded region. The measured relative humidity is indicated in the blue trace. The blue diamonds show the calculated particle extraction (%) from Eq. 2.

Figure 4 shows an intercomparison of the detection frequencies and normalized signal intensities from the hourly-averaged palmitic acid, glycerol, and K^+ data presented in Fig. 2 for each RH range, considering the full measurement period. Despite the effects on their signal intensities due to changing biological activity, the most significant and reproducible impact was due to sample RH. In Fig. 4A, we present the fraction of the hourly-averaged samples detected above background. Detection frequencies increased for all three ions with increasing RH, with glycerol demonstrating the most substantial increase from ~0% detection frequency at 20% RH to 100% detection frequency at 70% RH. In contrast to glycerol, K^+ and palmitic acid were still detected in about half of the measurements at 20% RH. These trends also held in terms of their normalized signal intensities shown as averages at the different RH ranges in Fig. 4B. Both glycerol and palmitic acid exhibited significantly greater average ion intensities with increasing RH across the bloom. In comparison, K^+ showed some but insignificant enhancement in signal with increasing RH.

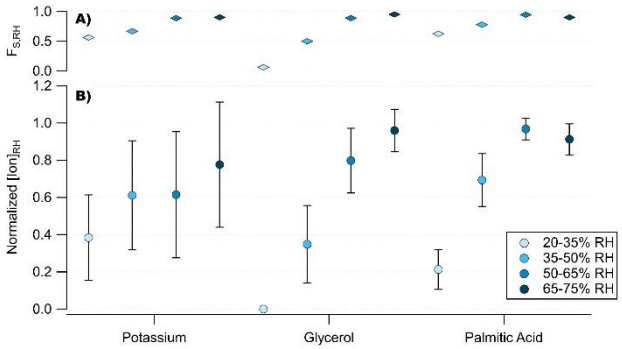

Figure 4. Variations in (A) detection frequency and (B) average normalized intensities of potassium, glycerol, and palmitic acid at different sample relative humidity ranges. Error bars represent the standard deviation of N=11, N=8, and N=12 hours of averaged data points in each RH range for potassium, glycerol, and palmitic acid, respectively, that were statistically significantly above the background. No error bar is shown for glycerol between a RH of 20% and 35% because there was only one hourly-averaged data point statistically significantly above the background level in that range.

In the study by Lopez-Hilfiker et al. 2019 using EESI-TOF, insignificant perturbations in the MS intensities were observed for homogeneously nucleated alpha-pinene secondary organic aerosol (SOA) components in the RH range between 0% and 80%, with most showing no perturbation at all.[44] We hypothesize that the change in RH can influence EESI-TOF sensitivity primarily in two ways: (1) the change in RH modulates the particle size of mostly water-soluble or hygroscopic aerosol particles, i.e., "shrinking" the particles with decreasing RH and "growing" the particles with increasing RH, affecting the coagulation efficiency between the sample aerosol particles and electrospray droplets, and (2) RH-induced phase transitions that modulate the aerosol's sticking probability or coagulation efficiency with the droplets and distance that components in the sample aerosol and the reagent ion (e.g., Na^+) in the electrospray droplet must diffuse before they interact. These two pathways are explored further in the following sections.

Particle Size Effects

As depicted in Figure S5, throughout the study, the surface area-weighted diameter varied with RH, ranging from 180(±10) nm to 239(±15) nm across the phytoplankton bloom, generally exhibiting a stepwise decrease in diameter between the highest and lowest RH. In Gallimore and Kalberer, 2013, the EESI-TOF response to components in purely organic aerosol particles was linear for particles with mobility diameters ranging from 70 nm to 200 nm.[46] In contrast, Lee et al. 2021 reported a significant and non-linear increase in the EESI-TOF sensitivity as the particle diameter decreased from 300 nm to 30 nm for organic-coated NH_4NO_3 particles.[53] They attributed the heightened sensitivity for smaller particles to differences in the coagulation rates between the sample aerosol particles and electrospray droplets, estimated from the Brownian coagulation coefficient,[91] calculating a coefficient of ~1 for 100 nm particles and ~10 for 30 nm particles. This translated to a 30x increase in sensitivity for the 30 nm particles compared to the 100 nm particles in that study. Furthermore, the coagulation coefficient varies dramatically and decreases above 100 nm. It is proposed that this variation is due to a reduced coagulation rate between the electrospray droplets (ranging from 0.5 to 5 μm) with larger sample aerosol and that a decrease in the difference between the size of the electrospray and the aerosol sample leads to a reduced coagulation rate. Without direct measurement of the electrospray droplet size distribution, these impacts remain unknown for other EESI-TOF measurements. However, based on the results in Lee et al. 2021, 200 nm particles, approximately the size of the peak number-weighted SSA particles measured here, have one to three times lower coagulation efficiency than 100 nm particles.[53] In this study, the decrease in the sample aerosol particle size at the lower RH is expected to enhance sensitivity because of the greater anticipated coagulation efficiency between smaller aerosol particles and larger electrospray droplets. Despite the anticipated increase in sensitivity with decreasing particle size

with lower RH, the opposite is observed – a marked decrease in sensitivity for most aerosol components at the lower RH. This suggests that the change in particle size with RH was either too small to influence coagulation rates significantly or that another RH-dependent mechanism is responsible.

Viscosity effects

A different explanation is the increased mobility of reactants resulting from the reduced SSA particle viscosity at higher RH.[22, 40, 52] This would heighten diffusive mixing and facilitate interactions between Na^+ at the particle surface and the molecular components in nascent SSA, akin to the enhanced reaction probabilities between molecules at the particle interface and in the bulk of lower viscosity aerosols at higher RH.[63, 92-94]

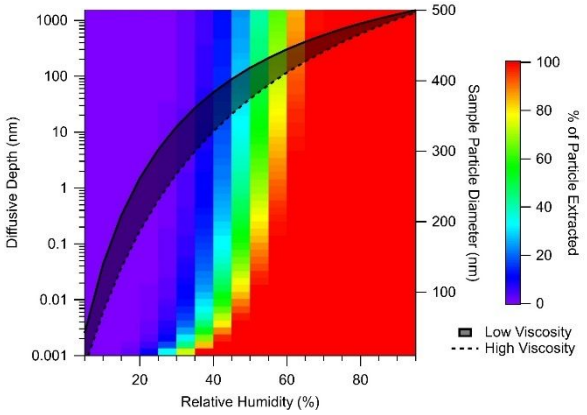

Figure 5. Modeled diffusive depths of the reagent ion, Na^+, in SSA particles at different particle diameters and as a function of relative humidity according to the relative humidity-dependent SSA viscosities reported in Tumminello et al., 2021, which was conducted jointly with this study. The color scale is the estimated percent particle volume extracted according to Eq. 2.

To examine the influence of RH-dependent viscosities on the diffusion and reaction between the Na^+ reagent ion and components in the particle phase, we modeled the "diffusive depth" of Na^+ entering an SSA particle between an RH of 5% to 95% in Fig. 5. The modeled diffusive depth represents the solution to the Stokes-Einstein equation under the assumption of atomic radii for Na^+ and the maximum residence time of a particle within the EESI-TOF inlet, as shown in Eq. 1:

$$Depth = \sqrt{t * \frac{k_b T}{6\pi\eta r}} \text{ (Eq. 1)}$$

Here, t represents the residence time inside the EESI-TOF inlet (16.96 milliseconds), k_b is the Boltzmann constant, T is the ambient temperature (K), η is the particle viscosity (Pa·s) estimated from Tumminello et al. 2021 for SSA, and r is the ionic radius of Na^+ of 1.02×10^{-10} m. η of SSA was taken directly from the estimated η for the organic carbon reported in Tumminello et al. 2021.[52] On the higher end, the η of SSA was estimated to range from 9.14×10^{10} Pa·s at 5% RH to 1.88×10^{-3} Pa·s at 95% RH, coinciding with the peak in chlorophyll-a, and between 5.58×10^{9} Pa·s at 5% RH to 1.55×10^{-2} Pa·s at 95% RH on the lower end, during a period of low biological activity. Other particle properties, e.g., solubility, surface tension, morphology, mixing state, and localized differences in pH and concentration of other reactants between the particle surface and bulk might also play a role in the mass transfer of components.[95] Therefore, the reported diffusive depths are treated as estimates to demonstrate viscosity's effects on mass transfer. If components at the particle surface dissolve into the electrospray droplet upon collision with the droplet, the Na^+ ion will likely interact with and diffuse to greater depths in the particle than predicted by this model. The reported mixing depths may serve as a lower limit in such cases. Figure 5 illustrates these outcomes as a function of RH. At a relatively low RH of 20%, Na^+ is estimated to penetrate the particle only to within 1 nm from the surface (black curve), while at a relatively high RH of 70%, the depth is around 200 nm, i.e., diffusing completely through the sample particle in the time the particles spend in the EESI inlet. While the modeled diffusive depth is independent of the sample's particle size, fewer molecules in larger particles will interact with Na^+ than in smaller ones with the same viscosity. To illustrate these different size-related effects, we can estimate the percentage of the sample aerosol particle volume extracted for spherical particles (Eq. 2), approximating the thickness of the particle layer extracted as the diffusive depth.

$$\%\ Volume\ Extracted = \frac{r_s^3 - (r_s - d)^3}{r_s^3} * 100 \text{ (Eq. 2)}$$

In Eq. 2, r_s is the sample particle radius (nm), and d is the diffusive depth (nm). For a nascent SSA particle with a mobility diameter of 211.5±15.4 nm, the estimated percent volume of the particle extracted and ionized by Na^+ is ~1.8% at 25% RH and 100% at 70% RH. This closely follows the relative palmitic acid signal intensity trends with RH shown in Fig. 3A (blue diamonds). This implies that in this study's sample RH range and the size range of SSA, increasingly smaller volume fractions of the nascent SSA were extracted and measured by the EESI-TOF with decreasing RH and that the extraction depends on the viscosity.

Potential Combined Effects of Viscosity and Particle Morphology on the Coagulation Efficiency and Extraction of Palmitic Acid, Glycerol, and K^+ in SSA

The ionization of glycerol and palmitic acid in SSA by EESI necessitated Na^+-adduct formation. Due to the lower η of SSA at elevated RH, we attribute the heightened detection frequencies at the higher RH to greater diffusivity and mixing of Na^+ with glycerol and palmitic acid. In addition, the less viscous, or stickier, SSA particles are expected to exhibit less bounce off and, thus, greater coagulation efficiency with the electrospray droplets with increasing RH,[96-98] promoting interactions between the molecules and reagent ion during EESI. As shown in Fig. S8, within the post-bloom period (between 8/5 and 8/9), the measured SSA particle bounce fractions, a proxy for particle viscosity,[52] were inversely proportional to the normalized intensities of all three ions. Within the peak bloom period (8/2 to 8/5), the highest normalized intensities coincided with the minimum bounce fraction and the smallest with the maximum bounce fraction. Although no clear or robust dependence between signal intensity and bounce fraction absolute values could be made, these results further indicate that less bouncy or stickier SSA particles yield higher detection frequencies and signal intensities with EESI-TOF compared to their bouncier counterparts at a lower RH.

Furthermore, particle morphologies were investigated with atomic force microscopy during SeaSCAPE for the same bloom, demonstrating an increasing number of larger core-shell SSA particles with solid-like organic shells across the bloom at the lower RH of 20% compared to an RH of 60%.[40] Such phase separation is common in SSA[22, 40, 56, 99] and may facilitate interactions between molecules at the particle surface and the EESI reagent ion. The observation that EESI demonstrates greater specificity for extracting and ionizing molecular components at the particle surface is not novel. Kumbhani et al. 2018 found minimal signal for $NaNO_3$ in the particle core and mostly glutaric acid from the particle surface for $NaNO_3$ particles coated with glutaric acid.[55] However, a substantial sampling of malonic acid and the glutaric acid core occurred, with malonic acid coating on glutaric acid particles.[55] As a surfactant, palmitic acid has a greater surface activity than glycerol, which could explain the higher detection frequencies for palmitic acid than glycerol at the lower RH. By a different mechanism, K^+ can be enriched at the surface of nascent SSA.[24, 100] Because K^+ is already ionized and does not require Na^+ ions to diffuse within the particle and react, less change in the K^+ signal intensity with RH was observed.

CONCLUSIONS

This study demonstrates the capability of the EESI-TOF method for measuring components in nascent SSA, namely palmitic acid, glycerol, and K^+. The finer temporal resolution enabled key new findings in our understanding of SSA molecular composition: (1) K^+ in SSA correlated with bacteria levels in seawater, possibly from complexation with anions in the DOC, and did not correlate with chlorophyll-a, (2) palmitic acid did not strongly correlate with either chlorophyll-a or bacterial cell counts but generally decreased in intensity as the chlorophyll-a concentrations in seawater decreased, and (3) glycerol correlated with chlorophyll-a, decreasing with time after the lamps were turned off. The different K^+, palmitic acid, and glycerol levels in SSA at different bloom periods could be important for understanding the evolution of SSA CCN activity throughout the bloom. Glycerol and other polyols are relatively hygroscopic organic compounds.[101] While palmitic acid is poorly soluble in water, it is surface active and, hence, expected to increase CCN activity via the Kelvin effect by suppressing the droplet's surface tension. In Tumminello et al., 2021, we observed this effect where the SSA CCN activity remained elevated even with a greater organic carbon mass fraction during the peak of the phytoplankton bloom.[6]

The impact of RH on sample extraction via the EESI-TOF method is significant, depending on the sample aerosol's size, viscosity, and morphology. Within the context of SSA, imaging of different authentic SSA particles has demonstrated that phase separation occurs in SSA in as many as six multistep phase transitions upon changes in RH.[22, 56] EESI extraction depends upon the ambient RH as shown here, and particle properties such as viscosity, and processes such as phase separation that depend on RH could critically impact the ability to detect molecular components by EESI-TOF, emphasizing the need for understanding the EESI extraction mechanism more precisely for different particle phases and multiple phases together. Phase-separated or core-shell-type particles, like the mixed glutaric acid/$NaNO_3$ particles studied in Kumbhani et al., 2018, and those common to SSA at a low RH,[22, 40, 52, 56] favor the extraction of components from the particle surface. On the other hand, well-mixed and deliquesced organic carbon/aqueous electrolyte particles with low viscosity, such as the nascent SSA near the deliquescence RH of sea salt,[52] favor complete extraction and ionization of the particles. Future work should also focus on the role of phase in other aerosol systems, e.g., in SOA, which undergoes liquid-liquid and liquid-solid phase transitions depending on the aerosol's composition and ambient RH.[95, 102]

The impact of phase on EESI is expected to be more relevant in detecting components in larger particles when the particle diameter is greater than the diffusive depth of the reagent ion. In the case of SSA, this suggests that the components in film droplets, which are smaller than jet droplets,[18] potentially have a higher probability of complete extraction based on their smaller size, contingent on particle viscosity. Our results suggest that studies quantifying molecular components in ambient aerosols with EESI-TOF could be underestimated, mainly if the ambient RH is lower (or the particles are more viscous) than when calibrated. These results highlight the importance of knowing the aerosol sample's physicochemical properties (i.e., phase state, viscosity, and morphology) for meaningful analysis of the results.

ASSOCIATED CONTENT

Supporting Information

The Supporting Information is available free of charge on the ACS Publications website.

Time series of the sampling time frames and biological activity markers (Fig. S1), K^+/Na^+_{SSA} temporal profiles (Fig. S2), bulk seawater and SSML pH temporal profiles (Fig. S3), heat map of the relative signal intensity and relative signal error in identified peaks separated by RH (Fig. S4), correlation plots between identified peaks and chlorophyll-a and bacteria (Fig. S5), hourly-averaged particle size temporal profiles (Fig. S6), K^+ mass spectrum (Fig. S7), and K^+, glycerol, and palmitic acid normalized intensity changes with particle bounce fractions (Fig. S8), list of previously identified compounds in SSA (Table S1). (PDF)

AUTHOR INFORMATION

Corresponding Author

Jonathan H. Slade – *Department of Chemistry & Biochemistry, University of California San Diego, La Jolla, CA, 92093, United States*

Present Addresses

Samantha M. Kruse – *Department of Chemistry & Biochemistry, University of California San Diego, La Jolla, CA, 92093, United States*

Paul R. Tumminello – *Department of Chemistry & Biochemistry, University of California San Diego, La Jolla, CA, 92093, United States*

Alexia N. Moore – *Department of Chemistry & Biochemistry, University of California San Diego, La Jolla, CA, 92093, United States*

Christopher Lee – *Scripps Institution of Oceanography, La Jolla, CA, 92037, United States*

Kimberly A. Prather – *Department of Chemistry & Biochemistry, University of California San Diego, La Jolla, CA, 92093, United States; Scripps Institution of Oceanography, La Jolla, CA, 92037, United States*

Author Contributions

S.M.K. and J.H.S. conceptualized and wrote the paper. S.M.K. made the mass spectrometric measurements and conducted the data analysis. P.R.T. performed the viscosity calculations. A.N.M. analyzed the bulk water pH and helped edit the paper. C.L. and K.A.P. managed the SeaSCAPE campaign and helped with editing. J.H.S. supervised S.M.K. and P.R.T.

ACKNOWLEDGMENT

This study was funded by the Center for Aerosol Impacts on Chemistry of the Environment (CAICE), an NSF Center for Chemical Innovation (CHE-1801971). The authors thank the SeaSCAPE team for making the wave flume study possible. We thank Francesca Malfatti for providing chlorophyll-a and bacteria measurements, Daniel Crocker for SSML collection, and Kyle Angle for SSML pH measurements. We especially want to thank Kathryn Mayer, John Sauer, and Chris Cappa for their leadership in managing the daily activities of the wave flume.

REFERENCES

(1) Partanen, A. I.; Dunne, E. M.; Bergman, T.; Laakso, A.; Kokkola, H.; Ovadnevaite, J.; Sogacheva, L.; Baisnée, D.; Sciare, J.; Manders, A.; et al. Global modelling of direct and indirect effects of sea spray aerosol using a source function encapsulating wave state. *Atmos. Chem. Phys.* **2014**, *14* (21), 11731-11752.

(2) Partanen, A. I.; Kokkola, H.; others. Direct and indirect effects of sea spray geoengineering and the role of injected particle size. *Journal of* **2012**. DOI: 10.1029/2011JD016428.

(3) Ayash, T.; Gong, S.; Jia, C. Q. Direct and Indirect Shortwave Radiative Effects of Sea Salt Aerosols. *J. Clim.* **2008**, *21* (13), 3207-3220. DOI: 10.1175/2007JCLI2063.1 (acccessed 2024/2/18).

(4) Moore, M. J. K.; Furutani, H.; Roberts, G. C.; Moffet, R. C.; Gilles, M. K.; Palenik, B.; Prather, K. A. Effect of organic compounds on cloud condensation nuclei (CCN) activity of sea spray aerosol produced by bubble bursting. *Atmos. Environ.* **2011**, *45* (39), 7462-7469. DOI: 10.1016/j.atmosenv.2011.04.034.

(5) DeMott, P. J.; Hill, T. C. J.; McCluskey, C. S.; Prather, K. A.; Collins, D. B.; Sullivan, R. C.; Ruppel, M. J.; Mason, R. H.; Irish, V. E.; Lee, T.; et al. Sea spray aerosol as a unique source of ice nucleating particles. *Proc. Natl. Acad. Sci. U. S. A.* **2016**, *113* (21), 5797-5803. DOI: 10.1073/pnas.1514034112.

(6) Collins, D. B.; Bertram, T. H.; Sultana, C. M.; Lee, C.; Axson, J. L.; Prather, K. A. Phytoplankton blooms weakly influence the cloud forming ability of sea spray aerosol. *Geophys. Res. Lett.* **2016**, *43* (18), 9975-9983. DOI: 10.1002/2016gl069922.

(7) de Leeuw, G.; Andreas, E. L.; Anguelova, M. D.; Fairall, C. W.; Lewis, E. R.; O'Dowd, C.; Schulzl, M.; Schwartz, S. E. PRODUCTION FLUX OF SEA SPRAY AEROSOL. *Reviews of Geophysics* **2011**, *49*, 1-39. DOI: 10.1029/2010RG000349.

(8) Lewis, E. R.; Schwartz, S. E. *Sea Salt Aerosol Production: Mechanisms, Methods, Measurements, and Models*; American Geophysical Union, 2004.

(9) Grythe, H.; Ström, J.; Krejci, R.; Quinn, P.; Stohl, A. A review of sea-spray aerosol source functions using a large global set of sea salt aerosol concentration measurements. *Atmos. Chem. Phys.* **2014**, *14* (3), 1277-1297.

(10) Xu, W.; Ovadnevaite, J.; Fossum, K. N.; Lin, C.; Huang, R.-J.; Ceburnis, D.; O'Dowd, C. Sea spray as an obscured source for marine cloud nuclei. *Nat. Geosci.* **2022**, *15* (4), 282-286. DOI: 10.1038/s41561-022-00917-2 (acccessed 2024/3/2).

(11) Tsigaridis, K.; Koch, D.; Menon, S. Uncertainties and importance of sea spray composition on aerosol direct and indirect effects. *JGR Atmospheres*. DOI: 10.1029/2012JD018165.

(12) Ma, X.; Salzen, K.; Li, J. Modelling sea salt aerosol and its direct and indirect effects on climate. *Atmos. Chem. Phys.* **2007**, *8*, 1311-1327. DOI: 10.5194/ACP-8-1311-2008.

(13) Quinn, P. K.; Bates, T. S.; Miller, T. L.; Coffman, D. J.; Johnson, J. E.; Harris, J. M.; Ogren, J. A.; Forbes, G.; Anderson, T. L.; Covert, D. S.; et al. Surface submicron aerosol chemical composition: What fraction is not sulfate? *J. Geophys. Res.* **2000**, *105* (D5), 6785-6805. DOI: 10.1029/1999jd901034.

(14) Bertram, T. H.; Cochran, R. E.; Grassian, V. H.; Stone, E. A. Sea spray aerosol chemical composition: elemental and molecular mimics for laboratory studies of heterogeneous and multiphase reactions. *Chem. Soc. Rev.* **2018**, *47* (7), 2374-2400. DOI: 10.1039/c7cs00008a.

(15) Quinn, P. K.; Collins, D. B.; Grassian, V. H.; Prather, K. A.; Bates, T. S. Chemistry and related properties of freshly emitted sea spray aerosol. *Chem. Rev.* **2015**, *115* (10), 4383-4399. DOI: 10.1021/cr500713g.

(16) Patterson, J. P.; Collins, D. B.; Michaud, J. M.; Axson, J. L.; Sultana, C. M.; Moser, T.; Dommer, A. C.; Conner, J.; Grassian, V. H.; Stokes, M. D.; et al. Sea Spray Aerosol Structure and Composition Using Cryogenic Transmission Electron Microscopy. *ACS Cent Sci* **2016**, *2* (1), 40-47. DOI: 10.1021/acscentsci.5b00344.

(17) Ault, A. P.; Moffet, R. C.; Baltrusaitis, J.; Collins, D. B.; Ruppel, M. J.; Cuadra-Rodriguez, L. A.; Zhao, D.; Guasco, T. L.; Ebben, C. J.; Geiger, F. M.; et al. Size-dependent changes in sea spray aerosol composition and properties with different seawater conditions. *Environ. Sci. Technol.* **2013**, *47* (11), 5603-5612. DOI: 10.1021/es400416g.

(18) Wang, X.; Deane, G. B.; Moore, K. A.; Ryder, O. S.; Stokes, M. D.; Beall, C. M.; Collins, D. B.; Santander, M. V.; Burrows, S. M.; Sultana, C. M.; et al. The role of jet and film drops in controlling the mixing state of submicron sea spray aerosol particles. *Proc. Natl. Acad. Sci. U. S. A.* **2017**, *114* (27), 6978-6983. DOI: 10.1073/pnas.1702420114.

(19) Prather, K. A.; Bertram, T. H.; Grassian, V. H.; Deane, G. B.; Stokes, M. D.; Demott, P. J.; Aluwihare, L. I.; Palenik, B. P.; Azam, F.; Seinfeld, J. H.; et al. Bringing the ocean into the laboratory to probe the chemical complexity of sea spray aerosol. *Proc. Natl. Acad. Sci. U. S. A.* **2013**, *110* (19), 7550-7555. DOI: 10.1073/pnas.1300262110.

(20) O'Dowd, C. D.; Facchini, M. C.; Cavalli, F.; Ceburnis, D.; Mircea, M.; Decesari, S.; Fuzzi, S.; Yoon, Y. J.; Putaud, J.-P. Biogenically driven organic contribution to marine aerosol. *Nature* **2004**, *431* (7009), 676-680. DOI: 10.1038/nature02959.

(21) Crocker, D. R.; Hernandez, R. E.; Huang, H. D.; Pendergraft, M. A.; Cao, R.; Dai, J.; Morris, C. K.; Deane, G. B.; Prather, K. A.; Thiemens, M. H. Biological Influence on δ13C and Organic Composition of Nascent Sea Spray Aerosol. *ACS Earth Space Chem.* **2020**, *4* (9), 1686-1699. DOI: 10.1021/acsearthspacechem.0c00072.

(22) Lee, H. D.; Morris, H. S.; Laskina, O.; Sultana, C. M.; Lee, C.; Jayarathne, T.; Cox, J. L.; Wang, X.; Hasenecz, E. S.; DeMott, P. J.; et al. Organic Enrichment, Physical Phase State, and Surface Tension Depression of Nascent Core–Shell Sea Spray Aerosols during Two Phytoplankton Blooms. *ACS Earth Space Chem.* **2020**, *4* (4), 650-660. DOI: 10.1021/acsearthspacechem.0c00032.

(23) Jayarathne, T.; Sultana, C. M.; Lee, C.; Malfatti, F.; Cox, J. L.; Pendergraft, M. A.; Moore, K. A.; Azam, F.; Tivanski, A. V.; Cappa, C. D.; et al. Enrichment of Saccharides and Divalent Cations in Sea Spray Aerosol During Two Phytoplankton Blooms. *Environ. Sci. Technol.* **2016**, *50* (21), 11511-11520. DOI: 10.1021/acs.est.6b02988.

(24) Cochran, R. E.; Laskina, O.; Jayarathne, T.; Laskin, A.; Laskin, J.; Lin, P.; Sultana, C.; Lee, C.; Moore, K. A.; Cappa, C. D.; et al. Analysis of Organic Anionic Surfactants in Fine and Coarse Fractions of Freshly Emitted Sea Spray Aerosol. *Environ. Sci. Technol.* **2016**, *50* (5), 2477-2486. DOI: 10.1021/acs.est.5b04053.

(25) Kattner, G.; Gercken, G.; Eberlein, K. Development of lipids during a spring plankton bloom in the northern North Sea: I. Particulate fatty acids. *Mar. Chem.* **1983**, *14* (2), 149-162. DOI: 10.1016/0304-4203(83)90038-5.

(26) Angle, K. J.; Nowak, C. M.; Davasam, A.; Dommer, A. C.; Wauer, N. A.; Amaro, R. E.; Grassian, V. H. Amino Acids Are

Driven to the Interface by Salts and Acidic Environments. *J. Phys. Chem. Lett.* **2022**, *13* (12), 2824-2829. DOI: 10.1021/acs.jpclett.2c00231.

(27) Triesch, N.; van Pinxteren, M.; Salter, M.; Stolle, C.; Pereira, R.; Zieger, P.; Herrmann, H. Sea Spray Aerosol Chamber Study on Selective Transfer and Enrichment of Free and Combined Amino Acids. *ACS Earth Space Chem.* **2021**, *5* (6), 1564-1574. DOI: 10.1021/acsearthspacechem.1c00080.

(28) Ovadnevaite, J.; Ceburnis, D.; Martucci, G.; Bialek, J.; Monahan, C.; Rinaldi, M.; Facchini, M. C.; Berresheim, H.; Worsnop, D. R.; O'Dowd, C. Primary marine organic aerosol: A dichotomy of low hygroscopicity and high CCN activity. *Geophys. Res. Lett.* **2011**, *38* (21). DOI: 10.1029/2011gl048869.

(29) Westervelt, D. M.; Moore, R. H.; Nenes, A.; Adams, P. J. Effect of primary organic sea spray emissions on cloud condensation nuclei concentrations. *Atmos. Chem. Phys.* **2012**, *12* (1), 89-101. DOI: 10.5194/acp-12-89-2012 (acccessed 2024/3/2).

(30) Sixth Assessment Report. (acccessed 2024/2/29).

(31) Glicker, H. S.; Lawler, M. J.; Chee, S.; Resch, J.; Garofalo, L. A.; Mayer, K. J.; Prather, K. A.; Farmer, D. K.; Smith, J. N. Chemical Composition of an Ultrafine Sea Spray Aerosol during the Sea Spray Chemistry and Particle Evolution Experiment. *ACS Earth Space Chem.* **2022**. DOI: 10.1021/acsearthspacechem.2c00127.

(32) Franklin, E. B.; Amiri, S.; Crocker, D.; Morris, C.; Mayer, K.; Sauer, J. S.; Weber, R. J.; Lee, C.; Malfatti, F.; Cappa, C. D.; et al. Anthropogenic and Biogenic Contributions to the Organic Composition of Coastal Submicron Sea Spray Aerosol. *Environ. Sci. Technol.* **2022**. DOI: 10.1021/acs.est.2c04848.

(33) Cochran, R. E.; Jayarathne, T.; Stone, E. A.; Grassian, V. H. Selectivity Across the Interface: A Test of Surface Activity in the Composition of Organic-Enriched Aerosols from Bubble Bursting. *J. Phys. Chem. Lett.* **2016**, *7* (9), 1692-1696. DOI: 10.1021/acs.jpclett.6b00489.

(34) Sauer, J. S.; Mayer, K. J.; Lee, C.; Alves, M. R.; Amiri, S.; Bahaveolos, C. J.; Franklin, E. B.; Crocker, D. R.; Dang, D.; Dinasquet, J.; et al. The Sea Spray Chemistry and Particle Evolution Study (SeaSCAPE): Overview and Experimental Methods. *Environ. Sci. Process. Impacts* **2022**.

(35) Petras, D.; Koester, I.; Da Silva, R.; Stephens, B. M.; Haas, A. F.; Nelson, C. E.; Kelly, L. W.; Aluwihare, L. I.; Dorrestein, P. C. High-Resolution Liquid Chromatography Tandem Mass Spectrometry Enables Large Scale Molecular Characterization of Dissolved Organic Matter. *Frontiers in Marine Science* **2017**, *4*. DOI: 10.3389/fmars.2017.00405.

(36) Pendergraft, M. A.; Belda-Ferre, P.; Petras, D.; Morris, C. K.; Mitts, B. A.; Aron, A. T.; Bryant, M.; Schwartz, T.; Ackermann, G.; Humphrey, G.; et al. Bacterial and Chemical Evidence of Coastal Water Pollution from the Tijuana River in Sea Spray Aerosol. *Environ. Sci. Technol.* **2023**. DOI: 10.1021/acs.est.2c02312.

(37) Ault, A. P.; Zhao, D.; Ebben, C. J.; Tauber, M. J.; Geiger, F. M.; Prather, K. A.; Grassian, V. H. Raman microspectroscopy and vibrational sum frequency generation spectroscopy as probes of the bulk and surface compositions of size-resolved sea spray aerosol particles. *Phys. Chem. Chem. Phys.* **2013**, *15* (17), 6206-6214. DOI: 10.1039/c3cp43899f.

(38) Trueblood, J. V.; Wang, X.; Or, V. W.; Alves, M. R.; Santander, M. V.; Prather, K. A.; Grassian, V. H. The Old and the New: Aging of Sea Spray Aerosol and Formation of Secondary Marine Aerosol through OH Oxidation Reactions. *ACS Earth Space Chem.* **2019**, *3* (10), 2307-2314. DOI: 10.1021/acsearthspacechem.9b00087.

(39) Lewis, S. L.; Russell, L. M.; Saliba, G.; Quinn, P. K.; Bates, T. S.; Carlson, C. A.; Baetge, N.; Aluwihare, L. I.; Boss, E.; Frossard, A. A.; et al. Characterization of Sea Surface Microlayer and Marine Aerosol Organic Composition Using STXM-NEXAFS Microscopy and FTIR Spectroscopy. *ACS Earth Space Chem.* **2022**. DOI: 10.1021/acsearthspacechem.2c00119.

(40) Kaluarachchi, C. P.; Or, V. W.; Lan, Y.; Madawala, C. K.; Hasenecz, E. S.; Crocker, D. R.; Morris, C. K.; Lee, H. D.; Mayer, K. J.; Sauer, J. S.; et al. Size-Dependent Morphology, Composition, Phase State, and Water Uptake of Nascent Submicrometer Sea Spray Aerosols during a Phytoplankton Bloom. *ACS Earth Space Chem.* **2022**, *6* (1), 116-130. DOI: 10.1021/acsearthspacechem.1c00306.

(41) Kaluarachchi, C. P.; Or, V. W.; Lan, Y.; Hasenecz, E. S.; Kim, D.; Madawala, C. K.; Dorcé, G. P.; Mayer, K. J.; Sauer, J. S.; Lee, C.; et al. Effects of Atmospheric Aging Processes on Nascent Sea Spray Aerosol Physicochemical Properties. *ACS Earth Space Chem* **2022**, *6* (11), 2732-2744. DOI: 10.1021/acsearthspacechem.2c00258.

(42) Collins, D. B.; Zhao, D. F.; Ruppel, M. J.; Laskina, O.; Grandquist, J. R.; Modini, R. L.; Stokes, M. D.; Russell, L. M.; Bertram, T. H.; Grassian, V. H.; et al. Direct aerosol chemical composition measurements to evaluate the physicochemical differences between controlled sea spray aerosol generation schemes. *Atmos. Meas. Tech. Discuss.* **2014**, *7* (7), 6457-6499. DOI: 10.5194/amtd-7-6457-2014.

(43) Sultana, C. M.; Collins, D. B.; Prather, K. A. Effect of Structural Heterogeneity in Chemical Composition on Online Single-Particle Mass Spectrometry Analysis of Sea Spray Aerosol Particles. *Environ. Sci. Technol.* **2017**, *51* (7), 3660-3668. DOI: 10.1021/acs.est.6b06399.

(44) Lopez-Hilfiker, F. D.; Pospisilova, V.; others. An extractive electrospray ionization time-of-flight mass spectrometer (EESI-TOF) for online measurement of atmospheric aerosol particles. *Atmospheric* **2019**.

(45) Law, W. S.; Wang, R.; Hu, B.; Berchtold, C.; Meier, L.; Chen, H.; Zenobi, R. On the mechanism of extractive electrospray ionization. *Anal. Chem.* **2010**, *82* (11), 4494-4500. DOI: 10.1021/ac100390t.

(46) Gallimore, P. J.; Kalberer, M. Characterizing an extractive electrospray ionization (EESI) source for the online mass spectrometry analysis of organic aerosols. *Environ. Sci. Technol.* **2013**, *47* (13), 7324-7331. DOI: 10.1021/es305199h.

(47) Surdu, M.; Pospisilova, V.; Xiao, M.; Wang, M.; Mentler, B.; Simon, M.; Stolzenburg, D.; Hoyle, C. R.; Bell, D. M.; Lee, C. P.; et al. Molecular characterization of ultrafine particles using extractive electrospray time-of-flight mass spectrometry. *Environ Sci Atmos* **2021**, *1* (6), 434-448. DOI: 10.1039/d1ea00050k.

(48) Brown, W. L.; Day, D. A.; Stark, H.; Pagonis, D.; Krechmer, J. E.; Liu, X.; Price, D. J.; Katz, E. F.; DeCarlo, P. F.; Masoud, C. G.; et al. Real-time organic aerosol chemical speciation in the indoor environment using extractive electrospray ionization mass spectrometry. *Indoor Air* **2021**, *31* (1), 141-155. DOI: 10.1111/ina.12721.

(49) Chen, H.; Venter, A.; Cooks, R. G. Extractive electrospray ionization for direct analysis of undiluted urine, milk and other complex mixtures without sample preparation. *Chem. Commun.* **2006**, (19), 2042-2044. DOI: 10.1039/b602614a.

(50) Doezema, L. A.; Longin, T.; Cody, W.; Perraud, V.; Dawson, M. L.; Ezell, M. J.; Greaves, J.; Johnson, K. R.; Finlayson-Pitts, B. J. Analysis of secondary organic aerosols in air using extractive electrospray ionization mass spectrometry (EESI-MS). *RSC Adv.* **2012**, *2* (7), 2930-2938. DOI: 10.1039/C2RA00961G (acccessed 2022/10/13).

(51) Pagonis, D.; Campuzano-Jost, P.; Guo, H.; Day, D. A.; Schueneman, M. K.; Brown, W. L.; Nault, B. A.; Stark, H.; Siemens, K.; Laskin, A.; et al. Airborne extractive electrospray mass spectrometry measurements of the chemical composition of organic aerosol. *Atmos. Meas. Tech.* **2021**, *14* (2), 1545-1559. DOI: 10.5194/amt-14-1545-2021.

(52) Tumminello, P. R.; James, R. C.; Kruse, S.; Kawasaki, A.; Cooper, A.; Guadalupe-Diaz, I.; Zepeda, K. L.; Crocker, D. R.; Mayer, K. J.; Sauer, J. S.; et al. Evolution of Sea Spray Aerosol Particle Phase State Across a Phytoplankton Bloom. *ACS Earth Space Chem.* **2021**, *5* (11), 2995-3007. DOI: 10.1021/acsearthspacechem.1c00186.

(53) Lee, C. P.; Surdu, M.; Bell, D. M.; Lamkaddam, H.; Wang, M.; Ataei, F.; Hofbauer, V.; Lopez, B.; Donahue, N. M.; Dommen, J.; et al. Effects of aerosol size and coating thickness on the molecular detection using extractive electrospray ionization. *Atmospheric Measurement Techniques* **2021**, *14* (9), 5913-5923.

(54) Lee, C. P.; Surdu, M.; Bell, D. M.; Dommen, J.; Xiao, M.; Zhou, X.; Baccarini, A.; Giannoukos, S.; Wehrle, G.; Schneider, P.

A.; et al. High-frequency gaseous and particulate chemical characterization using extractive electrospray ionization mass spectrometry (Dual-Phase-EESI-TOF). *Atmospheric Measurement Techniques* **2022**, *15* (12), 3747-3760. DOI: 10.5194/amt-15-3747-2022 (acccessed 2024/2/19).

(55) Kumbhani, S.; Longin, T.; Wingen, L. M.; Kidd, C.; Perraud, V.; Finlayson-Pitts, B. J. New Mechanism of Extractive Electrospray Ionization Mass Spectrometry for Heterogeneous Solid Particles. *Anal. Chem.* **2018**, *90* (3), 2055-2062. DOI: 10.1021/acs.analchem.7b04164.

(56) Nandy, L.; Liu, S.; Gunsbury, C.; Wang, X.; Pendergraft, M. A.; Prather, K. A.; Dutcher, C. S. Multistep Phase Transitions in Sea Surface Microlayer Droplets and Aerosol Mimics using Microfluidic Wells. *ACS Earth Space Chem.* **2019**, *3* (7), 1260-1267. DOI: 10.1021/acsearthspacechem.9b00121.

(57) You, Y.; Smith, M. L.; Song, M.; Martin, S. T.; Bertram, A. K. Liquid–liquid phase separation in atmospherically relevant particles consisting of organic species and inorganic salts. *Int. Rev. Phys. Chem.* **2014**, *33* (1), 43-77. DOI: 10.1080/0144235X.2014.890786.

(58) Richards, D. S.; Trobaugh, K. L.; Hajek-Herrera, J.; Price, C. L.; Sheldon, C. S.; Davies, J. F.; Davis, R. D. Ion-molecule interactions enable unexpected phase transitions in organic-inorganic aerosol. *Sci Adv* **2020**, *6* (47). DOI: 10.1126/sciadv.abb5643.

(59) Franklin, E. B.; Alves, M. R.; Moore, A. N.; Kilgour, D. B.; Novak, G. A.; Mayer, K.; Sauer, J. S.; Weber, R. J.; Dang, D.; Winter, M.; et al. Atmospheric Benzothiazoles in a Coastal Marine Environment. *Environ. Sci. Technol.* **2021**, *55* (23), 15705-15714. DOI: 10.1021/acs.est.1c04422.

(60) Alves, M. R.; Coward, E. K.; Gonzales, D.; Sauer, J. S.; Mayer, K. J.; Prather, K. A.; Grassian, V. H. Changes in light absorption and composition of chromophoric marine-dissolved organic matter across a microbial bloom. *Environ. Sci. Process. Impacts* **2022**, *24* (10), 1923-1933. DOI: 10.1039/d2em00150k.

(61) DeMott, P. J.; Hill, T. C. J.; Moore, K. A.; Perkins, R. J.; Mael, L. E.; Busse, H. L.; Lee, H.; Kaluarachchi, C. P.; Mayer, K. J.; Sauer, J. S.; et al. Atmospheric oxidation impact on sea spray produced ice nucleating particles. *Environ. Sci.: Atmos.* **2023**. DOI: 10.1039/D3EA00060E (acccessed 2023/9/7).

(62) Wang, X.; Sultana, C. M.; Trueblood, J.; Hill, T. C. J.; Malfatti, F.; Lee, C.; Laskina, O.; Moore, K. A.; Beall, C. M.; McCluskey, C. S.; et al. Microbial Control of Sea Spray Aerosol Composition: A Tale of Two Blooms. *ACS Cent Sci* **2015**, *1* (3), 124-131. DOI: 10.1021/acscentsci.5b00148.

(63) Kruse, S. M.; Slade, J. H. Heterogeneous and Photosensitized Oxidative Degradation Kinetics of the Plastic Additive Bisphenol-A in Sea Spray Aerosol Mimics. *J. Phys. Chem. A* **2023**, *127* (21), 4724-4733. DOI: 10.1021/acs.jpca.3c00127.

(64) Pospisilova, V.; Lopez-Hilfiker, F. D.; Bell, D. M.; Haddad, I. E.; Mohr, C.; Huang, W.; Heikkinen, L.; Xiao, M.; Dommen, J.; Prevot, A. S. H.; et al. On the fate of oxygenated organic molecules in atmospheric aerosol particles. *Science Advances* **2020**, *6* (11), eaax8922. DOI: 10.1126/sciadv.aax8922.

(65) Stark, H.; Yatavelli, R. L. N.; Thompson, S. L.; Kimmel, J. R.; Cubison, M. J.; Chhabra, P. S.; Canagaratna, M. R.; Jayne, J. T.; Worsnop, D. R.; Jimenez, J. L. Methods to extract molecular and bulk chemical information from series of complex mass spectra with limited mass resolution. *Int. J. Mass Spectrom.* **2015**, *389*, 26-38. DOI: 10.1016/j.ijms.2015.08.011.

(66) Cochran, R. E.; Laskina, O.; Trueblood, J. V.; Estillore, A. D.; Morris, H. S.; Jayarathne, T.; Sultana, C. M.; Lee, C.; Lin, P.; Laskin, J.; et al. Molecular Diversity of Sea Spray Aerosol Particles: Impact of Ocean Biology on Particle Composition and Hygroscopicity. *Chem* **2017**, *2* (5), 655-667. DOI: 10.1016/j.chempr.2017.03.007.

(67) Decesari, S.; Paglione, M.; Rinaldi, M.; Dall'Osto, M.; Simó, R.; Zanca, N.; Volpi, F.; Facchini, M. C.; Hoffmann, T.; Götz, S.; et al. Shipborne measurements of Antarctic submicron organic aerosols: an NMR perspective linking multiple sources and bioregions. *Atmos. Chem. Phys.* **2020**, *20* (7), 4193-4207. DOI: 10.5194/acp-20-4193-2020.

(68) Facchini, M. C.; Rinaldi, M.; Decesari, S.; Carbone, C.; Finessi, E.; Mircea, M.; Fuzzi, S.; Ceburnis, D.; Flanagan, R.; Nilsson, E. D.; et al. Primary submicron marine aerosol dominated by insoluble organic colloids and aggregates. *Geophys. Res. Lett.* **2008**, *35* (17). DOI: 10.1029/2008gl034210.

(69) Huot, Y.; Babin, M.; Bruyant, F.; Grob, C.; Twardowski, M. S.; Claustre, H. Does chlorophyll a provide the best index of phytoplankton biomass for primary productivity studies? *Biogeosci. Discuss.* **2007**, *4* (2), 707-745. (acccessed 2024/1/11).

(70) Buchan, A.; LeCleir, G. R.; Gulvik, C. A.; González, J. M. Master recyclers: features and functions of bacteria associated with phytoplankton blooms. *Nat. Rev. Microbiol.* **2014**, *12* (10), 686-698. DOI: 10.1038/nrmicro3326.

(71) Budge, S. M.; Devred, E.; Forget, M.-H.; Stuart, V.; Trzcinski, M. K.; Sathyendranath, S.; Platt, T. Estimating concentrations of essential omega-3 fatty acids in the ocean: supply and demand. *ICES J. Mar. Sci.* **2014**, *71* (7), 1885-1893. DOI: 10.1093/icesjms/fsu003 (acccessed 2024/1/11).

(72) Yao, J.; Rock, C. O. Exogenous fatty acid metabolism in bacteria. *Biochimie* **2017**, *141*, 30-39. DOI: 10.1016/j.biochi.2017.06.015.

(73) Flores, J. M.; Bourdin, G.; Kostinski, A. B.; Altaratz, O.; Dagan, G.; Lombard, F.; Haëntjens, N.; Boss, E.; Sullivan, M. B.; Gorsky, G.; et al. Diel cycle of sea spray aerosol concentration. *Nat. Commun.* **2021**, *12* (1), 5476. DOI: 10.1038/s41467-021-25579-3.

(74) William C. Keene, M. S. L. J. S. R. A. A. F. D. J. K. J. R. M. L. M. R. J. D. K. P. K. Q. Factors That Modulate Properties of Primary Marine Aerosol Generated From Ambient Seawater on Ships at Sea. *Journal of Geophysical Research: Atmospheres* **2017**, *122* (21), 11,961-911,990. DOI: 10.1002/2017JD026872.

(75) Long, M. S.; Keene, W. C.; Kieber, D. J.; Frossard, A. A.; Russell, L. M.; Maben, J. R.; Kinsey, J. D.; Quinn, P. K.; Bates, T. S. Light-enhanced primary marine aerosol production from biologically productive seawater. *Geophys. Res. Lett.* **2014**, *41* (7), 2661-2670. DOI: 10.1002/2014gl059436.

(76) Liu, S.; Liu, C.-C.; Froyd, K. D.; Schill, G. P.; Murphy, D. M.; Bui, T. P.; Dean-Day, J. M.; Weinzierl, B.; Dollner, M.; Diskin, G. S.; et al. Sea spray aerosol concentration modulated by sea surface temperature. *Proc. Natl. Acad. Sci. U. S. A.* **2021**, *118* (9). DOI: 10.1073/pnas.2020583118.

(77) Lü, X.; Liu, X.; Xu, C.; Song, J.; Li, X.; Yuan, H.; Li, N.; Wang, D.; Yuan, H.; Ye, S. The origins and implications of glycerol ether lipids in China coastal wetland sediments. *Sci. Rep.* **2019**, *9* (1), 18529. DOI: 10.1038/s41598-019-55104-y.

(78) Fu, P.; Kawamura, K.; Miura, K. Molecular characterization of marine organic aerosols collected during a round-the-world cruise. *J. Geophys. Res.* **2011**, *116* (D13). DOI: 10.1029/2011jd015604.

(79) Savakis, P.; Tan, X.; Du, W.; Branco dos Santos, F.; Lu, X.; Hellingwerf, K. J. Photosynthetic production of glycerol by a recombinant cyanobacterium. *J. Biotechnol.* **2015**, *195*, 46-51. DOI: 10.1016/j.jbiotec.2014.12.015.

(80) Hellebust, J. A. Excretion of some organic compounds by marine phytoplankton1. *Limnol. Oceanogr.* **1965**, *10* (2), 192-206. DOI: 10.4319/lo.1965.10.2.0192.

(81) Suescún-Bolívar, L. P.; Iglesias-Prieto, R.; Thomé, P. E. Induction of glycerol synthesis and release in cultured Symbiodinium. *PLoS One* **2012**, *7* (10), e47182. DOI: 10.1371/journal.pone.0047182.

(82) Yao, Y.; Lu, Y.; Peng, K.-T.; Huang, T.; Niu, Y.-F.; Xie, W.-H.; Yang, W.-D.; Liu, J.-S.; Li, H.-Y. Glycerol and neutral lipid production in the oleaginous marine diatom Phaeodactylum tricornutum promoted by overexpression of glycerol-3-phosphate dehydrogenase. *Biotechnol. Biofuels* **2014**, *7* (1), 110. DOI: 10.1186/1754-6834-7-110.

(83) Ben-Amotz, A.; Sussman, I.; Avron, M. Glycerol production by Dunaliella. In *New Trends in Research and Utilization of Solar Energy through Biological Systems*, Mislin, H., Bachofen, R. Eds.; Birkhäuser Basel, 1982; pp 55-58.

(84) Poblete-Castro, I.; Wittmann, C.; Nikel, P. I. Biochemistry, genetics and biotechnology of glycerol utilization in Pseudomonas species. *Microb. Biotechnol.* **2020**, *13* (1), 32-53. DOI: 10.1111/1751-7915.13400.

(85) Tang, C. Y.; Allen, H. C. Ionic binding of Na+ versus K+ to the carboxylic acid headgroup of palmitic acid monolayers studied by vibrational sum frequency generation spectroscopy. *J. Phys. Chem. A* **2009**, *113* (26), 7383-7393. DOI: 10.1021/jp9000434.

(86) Salter, M. E.; Hamacher-Barth, E.; Leck, C.; Werner, J.; Johnson, C. M.; Riipinen, I.; Nilsson, E. D.; Zieger, P. Calcium enrichment in sea spray aerosol particles. *Geophys. Res. Lett.* **2016**, *43* (15), 8277-8285. DOI: 10.1002/2016gl070275.

(87) Louis, Y.; Garnier, C.; Lenoble, V.; Omanović, D.; Mounier, S.; Pizeta, I. Characterisation and modelling of marine dissolved organic matter interactions with major and trace cations. *Mar. Environ. Res.* **2009**, *67* (2), 100-107. DOI: 10.1016/j.marenvres.2008.12.002.

(88) Lu, Y.; Allen, H. E. Characterization of copper complexation with natural dissolved organic matter (DOM)--link to acidic moieties of DOM and competition by Ca and Mg. *Water Res.* **2002**, *36* (20), 5083-5101. DOI: 10.1016/s0043-1354(02)00240-3.

(89) Flynn, K. J.; Mitra, A. Feeding in mixoplankton enhances phototrophy increasing bloom-induced pH changes with ocean acidification. *J. Plankton Res.* **2023**, *45* (4), 636-651. DOI: 10.1093/plankt/fbad030.

(90) Hakim, A.; Suzuki, T.; Kobayashi, M. Strength of Humic Acid Aggregates: Effects of Divalent Cations and Solution pH. *ACS Omega* **2019**, *4* (5), 8559-8567. DOI: 10.1021/acsomega.9b00124.

(91) Davies, C. N. Coagulation of aerosols by brownian motion. *J. Aerosol Sci.* **1979**, *10* (2), 151-161. DOI: 10.1016/0021-8502(79)90064-8.

(92) Slade, J. H.; Knopf, D. A. Multiphase OH oxidation kinetics of organic aerosol: The role of particle phase state and relative humidity. *Geophys. Res. Lett.* **2014**, *41* (14), 5297-5306. DOI: 10.1002/2014gl060582.

(93) Rasool, Q. Z.; Shrivastava, M.; Liu, Y.; Gaudet, B.; Zhao, B. Modeling the Impact of the Organic Aerosol Phase State on Multiphase OH Reactive Uptake Kinetics and the Resultant Heterogeneous Oxidation Timescale of Organic Aerosol in the Amazon Rainforest. *ACS Earth Space Chem.* **2023**. DOI: 10.1021/acsearthspacechem.2c00366.

(94) Davies, J. F.; Wilson, K. R. Nanoscale interfacial gradients formed by the reactive uptake of OH radicals onto viscous aerosol surfaces. *Chem. Sci.* **2015**, *6* (12), 7020-7027. DOI: 10.1039/c5sc02326b.

(95) Schervish, M.; Donahue, N. M.; Shiraiwa, M. Effects of volatility, viscosity, and non-ideality on particle–particle mixing timescales of secondary organic aerosols. *Aerosol Sci. Technol.*, 1-16. DOI: 10.1080/02786826.2023.2256827.

(96) Rim, D.; Green, M.; Wallace, L.; Persily, A.; Choi, J.-I. Evolution of Ultrafine Particle Size Distributions Following Indoor Episodic Releases: Relative Importance of Coagulation, Deposition and Ventilation. *Aerosol Sci. Technol.* **2012**, *46* (5), 494-503. DOI: 10.1080/02786826.2011.639317.

(97) Wang, Y.; Chen, L.; Chen, R.; Tian, G.; Li, D.; Chen, C.; Ge, X.; Ge, G. Effect of relative humidity on the deposition and coagulation of aerosolized SiO2 nanoparticles. *Atmos. Res.* **2017**, *194*, 100-108. DOI: 10.1016/j.atmosres.2017.04.030.

(98) Yu, M.; Koivisto, A. J.; Hämeri, K.; Seipenbusch, M. Size Dependence of the Ratio of Aerosol Coagulation to Deposition Rates for Indoor Aerosols. *Aerosol Sci. Technol.* **2013**, *47* (4), 427-434. DOI: 10.1080/02786826.2012.759640.

(99) Xiao, H.-S.; Dong, J.-L.; Wang, L.-Y.; Zhao, L.-J.; Wang, F.; Zhang, Y.-H. Spatially Resolved Micro-Raman Observation on the Phase Separation of Effloresced Sea Salt Droplets. *Environ. Sci. Technol.* **2008**, *42* (23), 8698-8702. DOI: 10.1021/es801181f.

(100) Ault, A. P.; Guasco, T. L.; Ryder, O. S.; Baltrusaitis, J.; Cuadra-Rodriguez, L. A.; Collins, D. B.; Ruppel, M. J.; Bertram, T. H.; Prather, K. A.; Grassian, V. H. Inside versus outside: ion redistribution in nitric acid reacted sea spray aerosol particles as determined by single particle analysis. *J. Am. Chem. Soc.* **2013**, *135* (39), 14528-14531. DOI: 10.1021/ja407117x.

(101) Ekström, S.; Noziére, B.; Hansson, H. C. CCN Properties of Water-soluble Organic Compounds Produced by Common Bioaerosols. In Nucleation and Atmospheric Aerosols, 2007.

(102) Chen, Y.; Pei, X.; Liu, H.; Meng, Y.; Xu, Z.; Zhang, F.; Xiong, C.; Preston, T. C.; Wang, Z. Influence of acidity on liquid–liquid phase transitions of mixed secondary organic aerosol (SOA) proxy–inorganic aerosol droplets. *Atmos. Chem. Phys.* **2023**, *23* (17), 10255-10265. DOI: 10.5194/acp-23-10255-2023 (acccessed 2023/9/19).

Authors are required to submit a graphic entry for the Table of Contents (TOC) that, in conjunction with the manuscript title, should give the reader a representative idea of one of the following: A key structure, reaction, equation, concept, or theorem, etc., that is discussed in the manuscript. Consult the journal's Instructions for Authors for TOC graphic specifications.

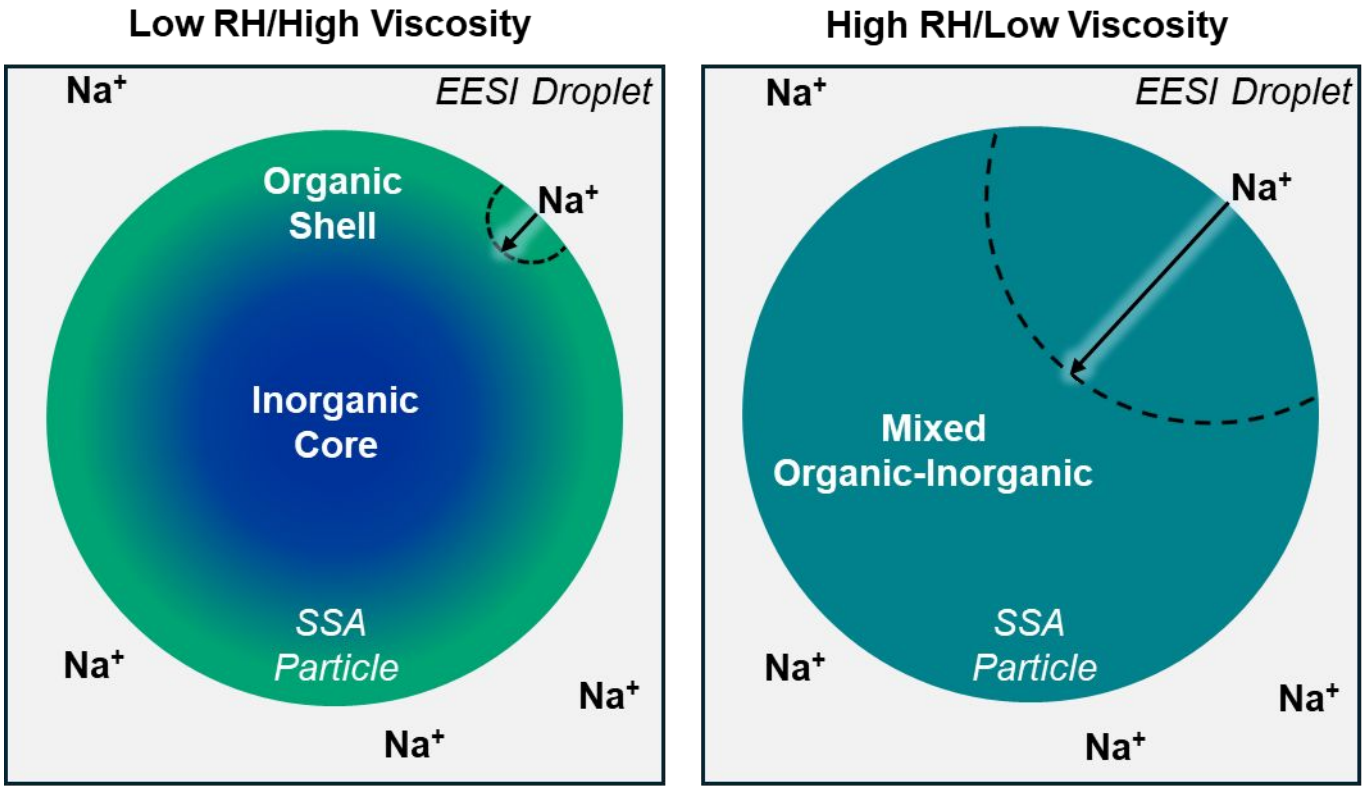

TOC Figure Caption: Different Na+ diffusive depths within particles with different morphologies and phase states. The left shows a shorter diffusive depth into a particle with a core-shell morphology and viscous outer organic layer at low relative humidity (RH) within an electrospray droplet. The right shows a longer diffusive depth into a well-mixed particle with a lower viscosity organic phase at a high RH.